

Particle swarm algorithm-based identification method of optimal measurement area of coordinate measuring machine

Cite as: Rev. Sci. Instrum. 95, 085105 (2024); doi: 10.1063/5.0206876

Submitted: 4 March 2024 • Accepted: 19 July 2024 •

Published Online: 8 August 2024



View Online



Export Citation



CrossMark

Hongfang Chen,^{a)} Huan Wu, Yi Gao, Zhaoyao Shi, Zhongpu Wen, and Ziqi Liang

AFFILIATIONS

Beijing Engineering Research Center of Precision Measurement Technology and Instruments, Beijing University of Technology, Beijing 100124, China

^{a)}Author to whom correspondence should be addressed: chf0302@126.com

ABSTRACT

A particle swarm algorithm-based identification method for the optimal measurement area of large coordinate measuring machines (CMMs) is proposed in this study to realize the intelligent identification of measurement objects and optimize the measurement position and measurement space using laser tracer multi-station technology. The volumetric error distribution of the planned measurement points in the CMM measurement space is obtained using laser tracer multi-station measurement technology. The volumetric error of the specified step distance measurement points is obtained using the inverse distance weighting (IDW) interpolation algorithm. The quasi-rigid body model of the CMM is solved using the LASSO algorithm to obtain the geometric error of the measurement points in a specified step. A model of individual geometric errors is fitted with least squares. An error optimization model for the measurement points in the CMM space is established. The particle swarm optimization algorithm is employed to optimize the model, and the optimal measurement area of the CMM airspace is determined. The experimental results indicate that, when the measurement space is optimized based on the volume of the object being measured, with dimensions of $(35 \times 35 \times 35) \text{ mm}^3$, the optimal measurement area for the CMM, as identified by the particle swarm algorithm, lies within the range of $150 \text{ mm} < X < 500 \text{ mm}$, $350 \text{ mm} < Y < 700 \text{ mm}$, and $-430 \text{ mm} < Z < -220 \text{ mm}$. In particular, the optimal measurement area is defined as $280 \text{ mm} < X < 315 \text{ mm}$, $540 \text{ mm} < Y < 575 \text{ mm}$, and $-400 \text{ mm} < Z < -365 \text{ mm}$. Comparative experiments utilizing a high-precision standard sphere with a diameter of 19.0049 mm and a sphericity of 50 nm demonstrate that the identified optimal measurement area is consistent with the results obtained through the particle swarm algorithm, thereby validating the correctness of the method proposed in this study.

Published under an exclusive license by AIP Publishing. <https://doi.org/10.1063/5.0206876>

24 October 2024 08:45:51

I. INTRODUCTION

A Coordinate Measuring Machine (CMM) serves as a highly efficient and precise measuring device in the field of coordinate measurement technology, capable of measuring the geometric characteristics of parts. It plays a crucial role in quality control within high-end precision manufacturing.^{1,2} The errors of a CMM primarily stem from factors such as mechanical issues, environmental influences, thermal deformation, and improper measurement methods. Based on the principle of spatial error similarity, errors at different measurement points within the entire measurement space of a CMM are correlated and exhibit continuous variation.^{3–5} There is an optimal measurement area in the CMM measurements. Placing

the object to be measured within this optimal area of the measuring machine can achieve high-precision measurements even with a CMM of lower accuracy. To accurately determine the precise location of the optimal measurement area in CMM, it is necessary to analyze the patterns of variation of the various error components and employ an appropriate optimization algorithm to find the exact location of the optimal measurement area in CMM.

Currently, both domestic and international scholars have focused their research on the optimal measurement area, primarily in the realms of articulated coordinate measuring machines and in-machine measurement systems for machine tools.^{6–8} The aim is to achieve high-precision measurement capabilities with these machines. Zheng *et al.*⁹ investigated the application limitations of

flexible CMM and established an error model based on the principles of functional networks and support vector regression machines, demonstrating the existence of an optimal measurement area. However, the establishment of this model relies solely on a large amount of actual measurement data, which limits its practicality. Hu *et al.*¹⁰ used an ant-colony algorithm to determine the optimal measurement area of an articulated-arm CMM and employed Monte Carlo theory and numerical methods to simulate and analyze the measurement space of the CMM, but did not use simulation experiments to verify the effectiveness of the method. Yang *et al.*¹¹ established a comprehensive error model and a circular surface measurement error model for an on-machine measurement system and proposed a beetle tentacle search particle swarm optimization algorithm for solving the optimal measurement area for circular surface measurement. Lee *et al.*¹² proposed an in-machine measurement method that uses an error synthesis model to deduce the linear relationship between geometric errors and measurement positions, optimizing measurement costs and time. However, this method has limitations as it fails to determine the optimal measurement area for equipment such as five-axis machine tools. Nevertheless, there is a scarcity of research on determining the optimal measurement area for CMM that uses orthogonal coordinate measurement methods.¹³ CMM based on the orthogonal coordinate measurement method has a large measurement space, many error sources, and complicated spatial error distribution patterns. Further research is needed to determine the optimal measurement area for CMM on this basis.

Herein, a particle swarm algorithm-based identification method for the optimal measurement area of CMM is proposed.^{14,15} Using the proposed method, the optimal measurement area of CMM can be determined, and subsequently, the quality of the products manufactured based on CMM measurement can be improved.

II. VOLUMETRIC ERROR MEASUREMENT OF MEASUREMENT POINTS BASED ON SPECIFIED STEP OF CMM

The shape of an object is determined by many spatial points; therefore, the measurement of any geometric element can be considered the measurement of spatial points. Therefore, accurate measurements of the point coordinates of an object are the basis for determining geometric shapes and errors. After a component to be measured is placed in the allowed measurement space of a CMM, the coordinates of a series of points on the surface of the product in three-dimensional (3D) space are accurately measured and then processed and fitted into different measurement elements, such as straight lines, circles, and spheres, such that the geometric data of the measured component, including the geometric size, shape, and position, can be obtained via mathematical operations.¹⁶ Therefore, the component quality is affected by the measurement accuracy of the CMM.

Using laser tracer multi-station measurement technology, the volumetric errors at the planned measurement points in the CMM measurement space can be measured.

A. Measurement principle of volumetric errors of CMM based on laser tracer multi-station measurement technology

We assumed that a laser tracer was used to measure n planned measurement points in the CMM measurement space at m stations.

The theoretical coordinates of n planned measurement points are $A_i(x_i, y_i, z_i)$, $i = 1, 2, 3, \dots, n$. The station coordinates of the laser tracer are $P_j(X_j, Y_j, Z_j)$, $j = 1, 2, 3, \dots, m$. The distance from the laser tracer at station j to the initial measurement point A_1 is d_j . The relative interference length of the cat's eye reflector during the measurement process is l_{ij} , meaning the distance between the laser tracer and the catadioptric reflector at each station. Using the formula for the distance between two points in 3D space, we obtain

$$\sqrt{(x_i - X_j)^2 + (y_i - Y_j)^2 + (z_i - Z_j)^2} = d_j + l_{ij}, \quad (1)$$

where i is the number of planned measurement points ($i = 1, 2, 3, \dots, n$) and j is the number of stations ($j = 1, 2, 3, \dots, m$).

Using the redundant measurement method, a laser-tracing multi-station measurement model was constructed using a laser-tracing instrument in a time-shifted station manner. The cat's eye reflector was mounted on the probe of the CMM such that its movement was synchronous with that of the probe. The beam reflected from the reflector was received by the laser tracer, which allowed the tracing measurement of the relative displacement between the cat's eye reflector and laser tracer station to be achieved.¹⁷

In order to solve the equation, the station coordinates of the laser tracer are $P_j(X_j, Y_j, Z_j)$, and the distance from the laser tracer at station j to the initial measurement point A_1 is d_j . The two are used as the unknown quantities for solving the equation, and the theoretical coordinates of the planned measurement points are $A_i(x_i, y_i, z_i)$ in the CMM measurement space are used as the known quantities for the equation. The objective function of the nonlinear least squares problem is established based on the multi-station measurement model of the laser tracer,

$$F_i(x_j) = F_i(X_j, Y_j, Z_j, d_j) \\ = \sqrt{(x_i - X_j)^2 + (y_i - Y_j)^2 + (z_i - Z_j)^2} - d_j - l_{ij}, \quad (2)$$

$$\min_{x \in R^n} f(x) = \frac{1}{2} \sum_{i=1}^n F_i^2(x) = \frac{1}{2} \|F(x)\|^2, \quad (3)$$

where R^n is the n -dimensional set of real numbers.

To obtain the coordinates of the laser tracer station $P_j(X_j, Y_j, Z_j)$ and the initial distance d_j , the system of nonlinear equations above was solved using the Levenberg–Marquardt (L–M) algorithm.¹⁸

The station coordinates of the laser tracer are $P_j(X_j, Y_j, Z_j)$ obtained from the above solution, and the distance from the laser tracer at station j to the initial measurement point A_1 is d_j , which is taken as known conditions. The actual value $A_i'(x_i', y_i', z_i')$ of the planned measurement points is $A_i(x_i, y_i, z_i)$, which is solved based on the laser tracking multi-station measurement model and the L–M algorithm. The objective function of the nonlinear least squares problem is established based on the multi-station measurement model of the laser tracer,

$$F_j(x_i) = F_j(x_i, y_i, z_i) \\ = \sqrt{(x_i - X_j)^2 + (y_i - Y_j)^2 + (z_i - Z_j)^2} - d_j - l_{ij}. \quad (4)$$

Using the L–M algorithm, the system of nonlinear equations was solved to obtain the coordinate values $A_i'(x_i', y_i', z_i')$ of the planned measurement points in the CMM measurement space.

The volumetric errors of the planned measurement points were obtained by substituting the coordinate values into the following equation:

$$\begin{bmatrix} \Delta x_i \\ \Delta y_i \\ \Delta z_i \end{bmatrix} = \begin{bmatrix} x'_i \\ y'_i \\ z'_i \end{bmatrix} - \begin{bmatrix} x_i \\ y_i \\ z_i \end{bmatrix}. \quad (5)$$

B. Volumetric errors of measurement points with specified step in CMM measurement space

A few CMM spatial measurement points were established. Volumetric errors at more measurement points could not be adequately obtained. After the volumetric errors of the planned measurement points were obtained, interpolation was performed to obtain the volumetric errors of more measurement points and the distribution pattern of the accurate volumetric errors.

The Inverse Distance Weighting (IDW) interpolation method usually adopts the following two schemes in its reference point selection strategy: (1) Fixed search radius: Take the point to be inserted as the center of the circle, set a fixed radius, and use the sampling points falling within the circle as reference points. However, the difficulty of this method lies in determining a suitable search radius for a spherical measurement space. (2) Reference point fixation: the N sampling points nearest to the point to be interpolated are selected as the reference point of the IDW interpolation method. This strategy is suitable for the case where the measurement space is more regular and the distribution of measurement points is more uniform.¹⁹

Based on the distribution patterns of the planned measurement points with fixed steps for an object to be measured as well as the volumetric errors of the measurement points mentioned in Sec. II A, the CMM measurement space for the regular rectangular and measurement point distribution is more uniform. So the reference point fixed strategy for the IDW interpolation method²⁰ is to obtain the volumetric errors of the measurement points with a specified step.

III. GEOMETRIC ERRORS OBTAINED BY SOLVING QUASI-RIGID BODY MODEL USING LASSO ALGORITHM

Each linear axis of the CMM includes six geometric error components. Owing to the non-orthogonality among the three axes, three perpendicularity error components were indicated. Therefore, the CMM included 21 geometric error components. To solve the geometric errors, a quasi-rigid body model of the CMM was established. The established quasi-rigid body model differs depending on the CMM type. CMM structures are classified based on the different motion orders of the X-, Y-, and Z-axes. If the first, second, and third motions are along the X-, Y-, and Z-axes directions, respectively, then the motion relationship is of XYZ type, and six motion relationships exist: XYZ, XZY, YXZ, YZX, ZXY, and ZYX. The letter added before F in each motion relationship represents the motion direction of the workpiece. The letter added after F in each motion relationship represents the motion direction of the measuring machine. Therefore, each motion relationship involves four different models

of workpiece-measuring machine motion. For example, an XYZ-type motion relationship involves four types of motion models: FXYZ, XYFZ, XYFZ, and XYZF. In total, 24 quasi-rigid body models of the CMM were obtained. The mathematical modeling is different for different quasi-rigid body models. In this study, using the FYXZ CMM as an example, a quasi-rigid-body model was established as follows:

$$\begin{aligned} \Delta x &= \delta_x(x) + \delta_x(y) + \delta_x(z) - \alpha_{xz} \cdot z - \varepsilon_z(x) \cdot y + [\varepsilon_y(x) + \varepsilon_y(y)] \cdot z \\ &\quad - [\varepsilon_z(x) + \varepsilon_z(y) + \varepsilon_z(z)] \cdot y_p + [\varepsilon_y(x) + \varepsilon_y(y) + \varepsilon_y(z)] \cdot z_p, \end{aligned} \quad (6)$$

$$\begin{aligned} \Delta y &= \delta_y(x) + \delta_y(y) + \delta_y(z) - \alpha_{xy} \cdot x - \alpha_{yz} \cdot z + \varepsilon_z(y) \cdot x \\ &\quad - [\varepsilon_x(x) + \varepsilon_x(y)] \cdot z + [\varepsilon_z(x) + \varepsilon_z(y) + \varepsilon_z(z)] \cdot x_p \\ &\quad - [\varepsilon_x(x) + \varepsilon_x(y) + \varepsilon_x(z)] \cdot z_p, \end{aligned} \quad (7)$$

$$\begin{aligned} \Delta z &= \delta_z(x) + \delta_z(y) + \delta_z(z) + \varepsilon_y(y) \cdot x - [\varepsilon_y(x) + \varepsilon_y(y) + \varepsilon_y(z)] \cdot x_p \\ &\quad + [\varepsilon_x(x) + \varepsilon_x(y) + \varepsilon_x(z)] \cdot y_p, \end{aligned} \quad (8)$$

where (x_p, y_p, z_p) is the coordinate of the probe in the CMM table coordinate system; after moving y in the Y -axis, there exists a positioning error $\delta_y(y)$ with straightness motion errors $\delta_x(y)$ and $\delta_z(y)$; after the slide moves x in the X -axis, there exists a positioning error $\delta_x(x)$, straightness motion errors $\delta_y(x)$ and $\delta_z(x)$, with perpendicularity error α_{xy} ; after the spindle moves z along the Z -axis, there exists a positioning error $\delta_z(z)$, straightness motion errors $\delta_x(z)$, $\delta_y(z)$ with perpendicularity errors α_{yz} , α_{xz} ; $\varepsilon_x(x)$, $\varepsilon_y(x)$, $\varepsilon_z(x)$ are the roll, pitch, and yaw errors of the X -axis; $\varepsilon_y(y)$, $\varepsilon_x(y)$, $\varepsilon_z(y)$ are the roll, pitch, and yaw errors of the Y -axis; and $\varepsilon_z(z)$, $\varepsilon_x(z)$, $\varepsilon_y(z)$ are the roll, pitch, and yaw errors of the Z -axis.

Based on a previous study,²¹ the Least Absolute Shrinkage and Selection Operator (LASSO) algorithm was used to solve the quasi-rigid body model [Eqs. (6)–(8)]. The coefficients of the four angular errors $[\varepsilon_z(x), \varepsilon_x(z), \varepsilon_y(z), \text{ and } \varepsilon_z(z)]$ were composed of the coordinates of the initial measurement points, and the starting point of the quasi-rigid body model established in this study was $(0,0,0)$. Therefore, only 17 geometric error components were obtained using the LASSO algorithm.

IV. ESTABLISHMENT OF ERROR MODEL OF MEASUREMENT POINTS IN CMM SPACE

A. Individual geometric error modeling of CMM

The measurement errors at different locations in the measurement space are required to model the combined CMM errors and determine the optimal measurement area of the CMM. Considering that individual geometric errors are characterized by a small amount of data and a dynamic change in error data, a simple and easy-to-use polynomial fitting algorithm based on the least squares method is chosen. Individual geometric errors in the CMM are modeled and predicted.

The process of fitting a polynomial based on the least squares method is as follows:

For given individual geometric error data (p_i, G_i), it is assumed that it satisfies a t th degree polynomial,

$$G(p_i) = a_t p_i^t + a_{t-1} p_i^{(t-1)} + \dots + a_1 p_i + a_0, \quad (9)$$

where p_i is the displacement of the motion axis in the $x/y/z$ direction ($i = 1, 2, \dots, n$, where n is the number of planning measurement points); G_i is the actual value of an individual geometric error term corresponding to p_i ; for example, the positioning error $\delta_x(x)$ in the X -axis; $G(p_i)$ is the fitted individual geometric error term corresponding to p_i ; and a_k is the vector of coefficients of the fitting result ($k = 1, 2, \dots, t$, where t is the number of times of the fitting).

Compare the Sum of Squared Errors (SSEs) and the coefficient of determination R^2 for different numbers of fits to determine the optimal number of fits for the polynomial fit t . SSE and the coefficient of determination R^2 are given as follows:

$$SSE = \sum_{i=1}^n (G_i - G(p_i))^2, \quad (10)$$

$$SST = \sum_{i=1}^n (G_i - \bar{G}_i)^2, \quad (11)$$

$$R^2 = 1 - \frac{SSE}{SST}, \quad (12)$$

where SST is the total sum of squares, and \bar{G}_i is the mean of the actual values of the individual geometric error term corresponding to p_i . R^2 reflects the degree of fit of the regression straight line, which takes the value of $[0, 1]$. The closer R^2 tends to 1, the better the regression equation is fitted; and the closer R^2 tends to 0, the worse the regression equation is fitted.

In order to find the best value of the coefficient a_k of different orders, for each p_i , the sum of squares of the differences between the fitted values $G(p_i)$ and G_i computed by a t th order polynomial should be minimized, that is,

$$\begin{aligned} & \min \sum_{i=1}^n (G(p_i) - G_i)^2 \\ &= \min \sum_{i=1}^n (a_t p_i^t + a_{t-1} p_i^{(t-1)} + \dots + a_1 p_i + a_0 - G_i)^2. \end{aligned} \quad (13)$$

Using a_0, a_1, \dots, a_t as variables, a partial derivation of the above equation yields the $t+1$ set of equations,

$$\begin{bmatrix} n & \sum_{i=1}^n p_i & \dots & \sum_{i=1}^n p_i^t \\ \sum_{i=1}^n p_i & \sum_{i=1}^n p_i^2 & \dots & \sum_{i=1}^n p_i^{t+1} \\ \dots & \dots & \dots & \dots \\ \sum_{i=1}^n p_i^t & \sum_{i=1}^n p_i^{t+1} & \dots & \sum_{i=1}^n p_i^{2t} \end{bmatrix} \begin{bmatrix} a_0 \\ a_1 \\ \dots \\ a_t \end{bmatrix} = \begin{bmatrix} \sum_{i=1}^n G_i \\ \sum_{i=1}^n p_i G_i \\ \dots \\ \sum_{i=1}^n p_i^t G_i \end{bmatrix}. \quad (14)$$

This can be reduced to $MA = B$, then $A = M^{-1}B$, or the values of the individual coefficients a_k can be solved for by the elimination method, where

TABLE I. Positioning error data for the X -axis.

n	x (mm)	$\delta_x(x)$ (μm)	n	x (mm)	$\delta_x(x)$ (μm)	n	x (mm)	$\delta_x(x)$ (μm)
1	150	0	13	270	0.24	25	390	-0.36
2	160	1.00	14	280	0.08	26	400	-0.32
3	170	1.03	15	290	-0.04	27	410	-0.39
4	180	1.08	16	300	-0.17	28	420	-0.46
5	190	1.11	17	310	-0.23	29	430	-0.55
6	200	1.15	18	320	-0.30	30	440	-0.61
7	210	1.03	19	330	-0.38	31	450	-0.68
8	220	0.90	20	340	-0.44	32	460	-0.76
9	230	0.74	21	350	-0.50	33	470	-0.83
10	240	0.62	22	360	-0.46	34	480	-0.92
11	250	0.50	23	370	-0.43	35	490	-0.99
12	260	0.37	24	380	-0.39	36	500	-1.06

$$\begin{aligned} M &= \begin{bmatrix} n & \sum_{i=1}^n p_i & \dots & \sum_{i=1}^n p_i^t \\ \sum_{i=1}^n p_i & \sum_{i=1}^n p_i^2 & \dots & \sum_{i=1}^n p_i^{t+1} \\ \dots & \dots & \dots & \dots \\ \sum_{i=1}^n p_i^t & \sum_{i=1}^n p_i^{t+1} & \dots & \sum_{i=1}^n p_i^{2t} \end{bmatrix}, \\ A &= \begin{bmatrix} a_0 \\ a_1 \\ \dots \\ a_t \end{bmatrix}, \quad B = \begin{bmatrix} \sum_{i=1}^n G_i \\ \sum_{i=1}^n p_i G_i \\ \dots \\ \sum_{i=1}^n p_i^t G_i \end{bmatrix}. \end{aligned} \quad (15)$$

Based on the 17 geometric errors at a specified step obtained using the LASSO algorithm, the individual geometric errors of the CMM were modeled and predicted using the polynomial fitting modeling method based on least squares. The expressions for the positioning error, straightness error, and partial angular error fitting functions of the CMM along the X -, Y -, and Z -axes were obtained via polynomial fitting.

According to the polynomial fitting Eq. (9), the expression of the individual geometric error fitting function is obtained. The polynomial fitting is carried out by taking the positioning error $\delta_x(x)$ of the X -axis in the geometric error model solved based on the LASSO algorithm in Sec. III as an example. The positioning error data for the X -axis were obtained according to Sec. III of the study, which are shown in Table I.

The number of fits t , SSE, and the coefficient of determination R^2 are shown in Table II.

When polynomial fitting is performed for $t = 4$ times, the percentage of SSE reduction reaches 72.49%, and R^2 approximates 1. Considering that the larger the number of fitting times, the more complicated the computational steps are, therefore, in this study, $t = 4$ is chosen as the polynomial fitting order.

TABLE II. The number of fits t , SSE, and the coefficient of determination R^2 .

Number of fits t (times)	2	3	4
SSE (μm^2)	2.4417	2.2390	0.6173
Coefficient of determination R^2	0.8231	0.8401	0.9605

The positioning error data for the X-axis in Table I were substituted into Eq. (14) for polynomial fitting, and the results of the calculations are shown as follows:

$$\begin{bmatrix} 36 & 1170 & 4191000 & 1.6146 \times 10^9 & 6.5539 \times 10^{11} \\ 11700 & 4191000 & 1.6146 \times 10^9 & 6.5539 \times 10^{11} & 2.7615 \times 10^{14} \\ 4191000 & 1.6146 \times 10^9 & 6.5539 \times 10^{11} & 2.7615 \times 10^{14} & 1.1956 \times 10^{17} \\ 1.6146 \times 10^9 & 6.5539 \times 10^{11} & 2.7615 \times 10^{14} & 1.1956 \times 10^{17} & 5.2823 \times 10^{19} \\ 6.5539 \times 10^{11} & 2.7615 \times 10^{14} & 1.1956 \times 10^{17} & 5.2823 \times 10^{19} & 2.3706 \times 10^{22} \end{bmatrix} \begin{bmatrix} a_0 \\ a_1 \\ a_2 \\ a_3 \\ a_4 \end{bmatrix} = \begin{bmatrix} -1.3970 \\ -2.7625 \times 10^3 \\ -1.6464 \times 10^6 \\ -8.2027 \times 10^8 \\ -3.8711 \times 10^{11} \end{bmatrix}. \quad (16)$$

The solution is obtained by

$$\begin{cases} a_0 = -22.3733, \\ a_1 = 0.3366, \\ a_2 = -0.0017, \\ a_3 = 3.5756 \times 10^{-6}, \\ a_4 = -2.6846 \times 10^{-9}. \end{cases} \quad (17)$$

Substituting Eq. (17) with the polynomial fitting order $t = 4$ into Eq. (9) yields a model of the positioning error of the polynomial fitting to the X-axis,

$$\delta_x(x) = -2.6846 \times 10^{-9}x^4 + 3.5756 \times 10^{-6}x^3 - 0.0017x^2 + 0.3366x - 22.3733. \quad (18)$$

Similarly, the fitted function error model for the remaining 16 geometric errors can be obtained.

B. Error model of measurement point in CMM space

The established model of individual geometric errors was introduced into a quasi-rigid-body model [Eqs. (6)–(8)] established via coordinate transformation to obtain the expressions for the volumetric error functions Δx_i , Δy_i , and Δz_i . The error model for measurement points in the CMM space is expressed as follows:

$$E(x_i, y_i, z_i) = \sqrt{\Delta x_i^2 + \Delta y_i^2 + \Delta z_i^2}. \quad (19)$$

V. PARTICLE SWARM OPTIMIZATION (PSO) ALGORITHM-BASED DETERMINATION METHOD OF OPTIMAL MEASUREMENT AREA

A. Optimal measurement area model

The measurement errors of the CMM differ depending on the locations in the measurement space, which suggests the existence of an optimal measurement area. However, the optimal measurement area varies depending on the object to be measured. A measurement point error optimization model in a specified space was established to determine the maximum error of the measurement point. Subsequently, the maximum errors of the different measurement points were compared. The area with the smallest maximum error in the entire measurement space was regarded as the optimal measurement

area. The model for solving the maximum measurement point error in different measurement regions is expressed as follows:

$$\begin{cases} \min E(x_i, y_i, z_i) = \sqrt{\Delta x_i^2 + \Delta y_i^2 + \Delta z_i^2}, \\ \text{s.t. } x_{i\min} \leq x_i \leq x_{i\max}, \\ y_{i\min} \leq y_i \leq y_{i\max}, \\ z_{i\min} \leq z_i \leq z_{i\max}, \end{cases} \quad (20)$$

where $x_{i\min}$ and $x_{i\max}$ are the upper and lower bounds of the X-axis in different search regions, respectively; $y_{i\min}$ and $y_{i\max}$ are the upper and lower bounds of the Y-axis in different search regions, respectively; and $z_{i\min}$ and $z_{i\max}$ are the upper and lower bounds of the Z-axis in different search regions, respectively.

B. Particle swarm algorithm used to identify optimal measurement area for CMM

The PSO algorithm is a global optimization algorithm whose basic idea is to search for an optimal solution through collaboration and information sharing among individuals in a population. In the particle swarm algorithm, particles are used to simulate the behavior of birds to achieve better global search capability.²²

In this study, the particles represent errors in the measurement points at different locations in the CMM measurement space. The particles present only two attributes, i.e., velocity and position, which represent the search speed and direction, respectively. In identifying the optimal measurement area, a group of particles is randomly generated. After the maximum number of iterations is performed, the optimization speed, learning factor, inertia weight, and optimization bounds of the X-, Y-, and Z-axes are set, and each particle individually searches for the optimal solution of the measurement point error in the search space, which is then recorded as the current individual extremum and shared among the entire particle population.²³ Subsequently, the optimal individual extremum is obtained as the optimal solution for the current measurement point error in the entire measurement space. All the particles in the entire measurement space of the CMM adjust their velocity and position based on the current individual extremum and the optimal solution of the current measurement point error shared by the entire particle population. Finally, the optimal solution for the measurement point errors in the measurement space is obtained. The particle swarm algorithm (Fig. 1) is expressed as follows:

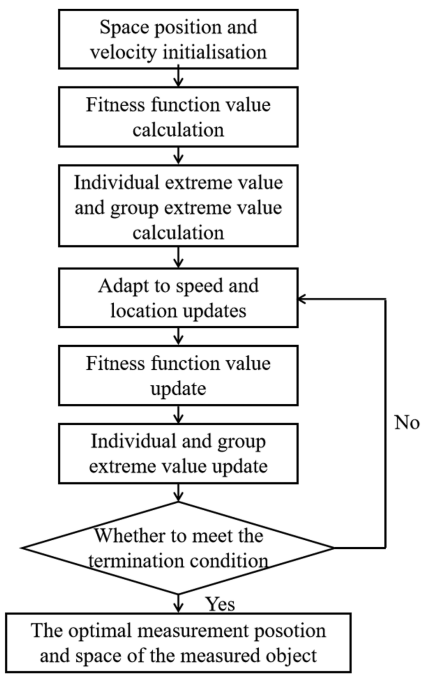


FIG. 1. Flow chart of the particle swarm algorithm.

The d -dimensional velocity update of particle i at each iteration is expressed as follows:

$$v_{id}^k = w v_{id}^{k-1} + c_1 r_1 (\text{pbest}_{id} - X_{id}^{k-1}) + c_2 r_2 (\text{gbest}_{id} - X_{id}^{k-1}). \quad (21)$$

The d -dimensional position update of particle i is expressed as follows:

$$X_{id}^k = X_{id}^{k-1} + v_{id}^{i-1}, \quad (22)$$

where v_{id}^k is the d -dimensional component of the velocity vector of particle i in the k th iteration, pbest denotes the current individual extremum, gbest denotes the current global optimal solution, X_{id}^k is the d -dimensional component of the position vector of particle i in the k th iteration, C_1 and C_2 are the acceleration constants used to regulate the maximum learning step, ω is the inertia weight with non-negative values, and r_1 and r_2 are two random functions of range $[0,1]$ for increasing the search randomness.

VI. EXPERIMENTS

The volumetric errors of the planned measurement points in the CMM measurement space were obtained via laser tracer-based multi-station measurement experiments. These step spacings were planned based on the measured object, and the volumetric errors of the measurement points in the CMM measurement space at the given step were obtained using the IDW interpolation algorithm. The LASSO algorithm was used to solve the quasi-rigid body model of the CMM to obtain the geometric errors of the measurement points at a specified step spacing. Subsequently, the least-squares

method combined with a quasi-rigid body model was used to establish a measurement point error model for identifying the optimal measurement area of the CMM.

After the optimal measurement area of the CMM was identified using the particle swarm algorithm with a standard sphere as the measured object, the measurement point errors were measured at different locations in the CMM measurement space to demonstrate the existence of the optimal measurement area. The standard sphere was placed at the location where the maximum errors of the measurement points in different regions were identified using the particle swarm algorithm to obtain the maximum errors of measurement points in different regions. Subsequently, the measured measurement errors were compared with the maximum errors of the measurement points in different regions identified using the particle swarm algorithm. Thus, the accuracy of the proposed method for identifying the optimal CMM measurement area was verified.

A. Experimental setup

A laser tracer multi-station measurement system is established (Fig. 2). Using redundant measurement methods, a multi-station measurement model is constructed using a single laser tracer with time-turning stations. The laser tracer is placed at different positions on the CMM measurement stage. The cat's eye reflector is fixed at the end of the CMM probe and moves with its probe.

The established optimal CMM measurement area verification platform (Fig. 3) was composed of a CMM (Hexagon Global 7.10.7) with a measurement range of $(700 \times 1000 \times 700) \text{ mm}^3$ and a high-precision standard sphere of (diameter = 19.0049 mm and precision = 50 nm). Due to the high position of the planned CMM measurement area, a combination of a magnetic base and a lifting platform was used to place the standard sphere within the planned measurement area. The combination of a magnetic base and lifting platform provides a height adjustment range of 100 to 230 mm. The height error of the magnetic base and the lifting platform is 0.9320 mm. The

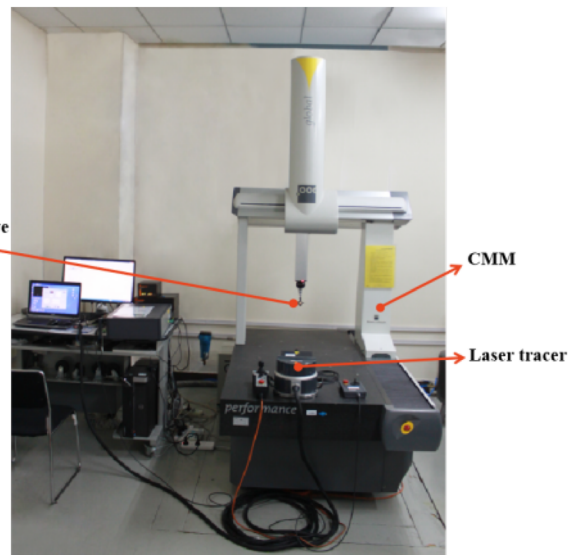


FIG. 2. Laser tracing multi-station measurement system.

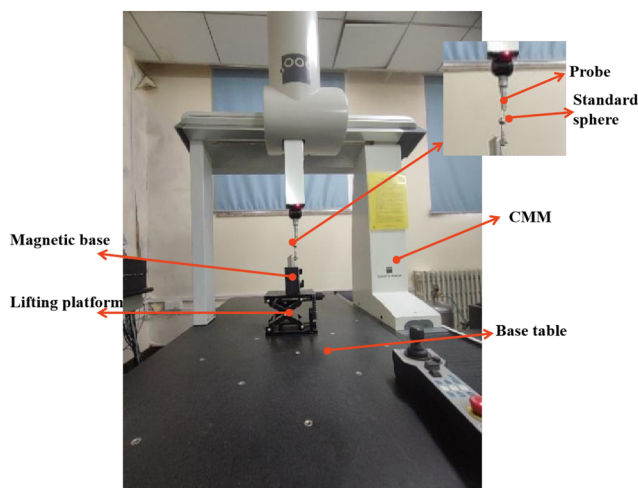


FIG. 3. Optimal CMM measurement area verification platform.

experimental environment was controlled at 20 °C. Under the guarantee of measurement accuracy and measurement integrity, it was stipulated that each measurement point took 5 s (from the beginning of the cat's eye movement to the completion of the measurement at rest).

B. Experimental results

1. Volumetric error of established measurement points on CMM using laser tracer multi-station measurement technology

In the CMM measurement space, a measurement space measuring $(350 \times 350 \times 210)$ mm³ was established. According to the planning, the measurement range of the X-axis is 150 mm $< x < 500$ mm with a step of 50 mm, the measurement range of the Y-axis is 350 mm $< y < 700$ mm with a step of 50 mm, and the measurement range of the Z-axis is $-430 \text{ mm} < z < -220$ mm with a step of 30 mm. A total of $8 \times 8 \times 8 = 512$ measurement points were established in the above-mentioned measurement space (Fig. 4). The laser tracer comprised four stations. The established measurement points and their volumetric errors were obtained using laser tracer multi-station measurement technology.

2. Volumetric errors of measurement points with specified step in CMM measurement space

The established three-coordinate space contained fewer measurement points. After the volumetric errors at the established points were obtained, those points were interpolated to obtain more measurement points and the corresponding volumetric errors to improve the accuracy of the geometric error solution. The interpolation step was performed based on the size of the measured object. If the interpolation step is smaller than that of the measured object, then the interpolation result is meaningless. In this study, the measured object was a standard sphere, and the interpolation step was

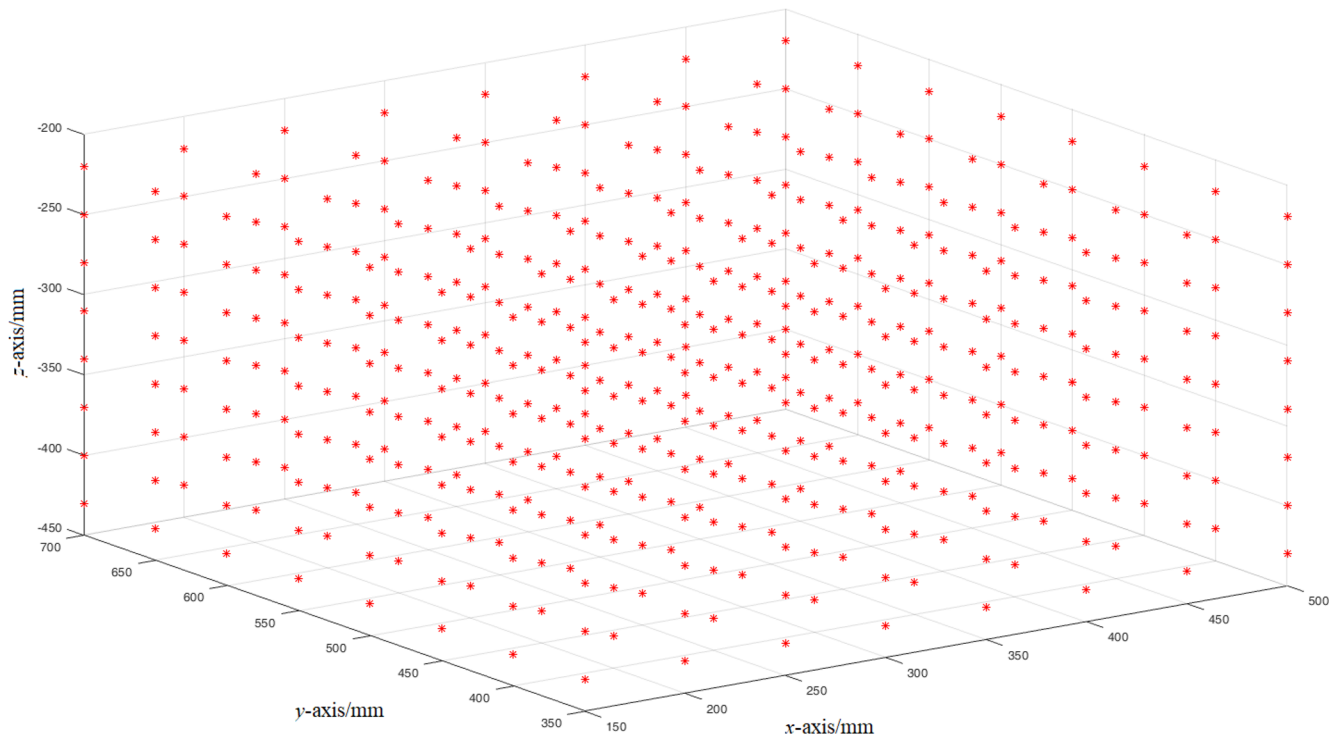


FIG. 4. Spatial distribution of established measurement points.

set at 10 mm. Each step in the entire CMM measurement space contained 28 512 measurement points. The volumetric errors at the measurement points at a specified step were obtained using the IDW interpolation method.

3. Setting of geometric errors of measurement points with specified step

The effects of the four roll angle errors [$\varepsilon_z(x)$, $\varepsilon_x(z)$, $\varepsilon_y(z)$, and $\varepsilon_z(z)$] on the volumetric errors were insignificant; hence, the four angular errors were negligible. The geometric errors obtained using the LASSO algorithm are shown in Fig. 5. Figure 5(a) shows the X-axis positioning and straightness errors; Fig. 5(b) shows the X-axis angular error; Fig. 5(c) shows the Y-axis positioning and straightness errors; Fig. 5(d) shows the Y-axis angular error; and Fig. 5(e) shows the Z-axis positioning and straightness errors. The verticality errors ($\alpha_{xy} = 0.001 \mu\text{rad}$, $\alpha_{yz} = 0.0026 \mu\text{rad}$, and $\alpha_{xz} = 0.003 \mu\text{rad}$) were solved using the LASSO algorithm.

4. Modeling individual geometric errors

The individual errors of the CMM did not vary linearly, and the variation of each individual error was different; therefore, the model for each individual error of the CMM was complex. Thus, the measurement errors differed depending on the locations in the CMM measurement space. The measurement errors at different locations were determined to model the combined CMM errors and the optimal measurement area of the CMM.

Based on the least-squares fitting theory in Sec. IV A and using the geometric errors of the measurement points with the specified step presented in Sec. VI B 3, the expressions of the individual geometric error functions of the CMM along the X-, Y-, and Z-axes were obtained.

The X-axis positioning error model is expressed as follows:

$$\delta_x(x) = -2.6846 \times 10^{-9}x^4 + 3.5756 \times 10^{-6}x^3 - 0.0017x^2 + 0.3366x - 22.3733. \quad (23)$$

The X-axis straightness error model is expressed as follows:

$$\delta_y(x) = -1.2768 \times 10^{-9}x^4 + 1.6607 \times 10^{-6}x^3 - 0.0008x^2 + 0.1564x - 10.7246. \quad (24)$$

The X-axis straightness error model is expressed as follows:

$$\delta_z(x) = -1.5145 \times 10^{-9}x^4 + 1.9312 \times 10^{-6}x^3 - 0.0009x^2 + 0.161x - 10.3072. \quad (25)$$

The X-axis angular motion error model is expressed as follows:

$$\varepsilon_x(x) = -5.4523 \times 10^{-12}x^4 + 7.1555 \times 10^{-9}x^3 - 3.3329x^2 + 0.0006x - 0.0428. \quad (26)$$

The X-axis angular motion error model is expressed as follows:

$$\varepsilon_y(x) = 7.1944 \times 10^{-12}x^4 - 1.0223 \times 10^{-8}x^3 + 5.2532 \times 10^{-6}x^2 - 0.0011x + 0.0788. \quad (27)$$

The Y-axis straightness error model is expressed as follows:

$$\begin{aligned} \delta_x(y) = & -4.3023 \times 10^{-10}y^4 + 9.1517 \times 10^{-7}y^3 \\ & - 0.0007y^2 + 0.2526y - 31.9906. \end{aligned} \quad (28)$$

The Y-axis positioning error model is expressed as follows:

$$\begin{aligned} \delta_y(y) = & 1.0887 \times 10^{-10}y^4 - 9.1033 \times 10^{-8}y^3 \\ & - 4.6389 \times 10^{-5}y^2 + 0.0565y - 11.6688. \end{aligned} \quad (29)$$

The Y-axis straightness error model is expressed as follows:

$$\begin{aligned} \delta_z(y) = & -1.6086 \times 10^{-10}y^4 + 6.8323 \times 10^{-7}y^3 \\ & - 0.0008y^2 + 0.3609y - 53.2079. \end{aligned} \quad (30)$$

The Y-axis angular motion error model is expressed as follows:

$$\begin{aligned} \varepsilon_x(y) = & -2.2513 \times 10^{-12}x^4 + 4.9906 \times 10^{-9}y^3 \\ & - 4.0742 \times 10^{-6}y^2 + 0.0014y - 0.1879. \end{aligned} \quad (31)$$

The Y-axis angular motion error model is expressed as follows:

$$\begin{aligned} \varepsilon_y(y) = & 7.8261 \times 10^{-13}y^4 - 1.1011 \times 10^{-9}y^3 \\ & + 4.5405 \times 10^{-7}y^2 - 3.9114 \times 10^{-5}y - 0.0049. \end{aligned} \quad (32)$$

The Y-axis angular motion error model is expressed as follows:

$$\begin{aligned} \varepsilon_z(y) = & 4.3787 \times 10^{-13}y^4 - 1.1175 \times 10^{-9}y^3 \\ & + 1.0311 \times 10^{-6}y^2 - 0.0004y + 0.0551. \end{aligned} \quad (33)$$

The Z-axis straightness error model is expressed as follows:

$$\begin{aligned} \delta_x(z) = & 3.8007 \times 10^{-9}z^4 + 4.1448 \times 10^{-6}z^3 \\ & + 0.0015z^2 + 0.2196z + 8.8303. \end{aligned} \quad (34)$$

The Z-axis straightness error model is expressed as follows:

$$\begin{aligned} \delta_y(z) = & 3.9227 \times 10^{-9}z^4 + 4.5562 \times 10^{-6}z^3 \\ & + 0.0019z^2 + 0.348z + 23.0267. \end{aligned} \quad (35)$$

The Z-axis positioning error model is expressed as follows:

$$\begin{aligned} \delta_z(z) = & -7.8935 \times 10^{-9}z^4 - 1.0114 \times 10^{-5}z^3 \\ & - 0.0048z^2 - 1.0088z - 79.0817. \end{aligned} \quad (36)$$

5. Verification of error model of measurement points in CMM space and error distribution pattern

The individual geometric error model established above was substituted into a quasi-rigid-body model [Eqs. (6)–(8)]. Subsequently, the quasi-rigid-body model was substituted into Eq. (19) to obtain the measurement-point error model. The measurement points with a specified step obtained using the IDW interpolation method were substituted into the measurement point error model to obtain the measurement point errors. The results were compared to those obtained using the IDW interpolation method (Fig. 6). The

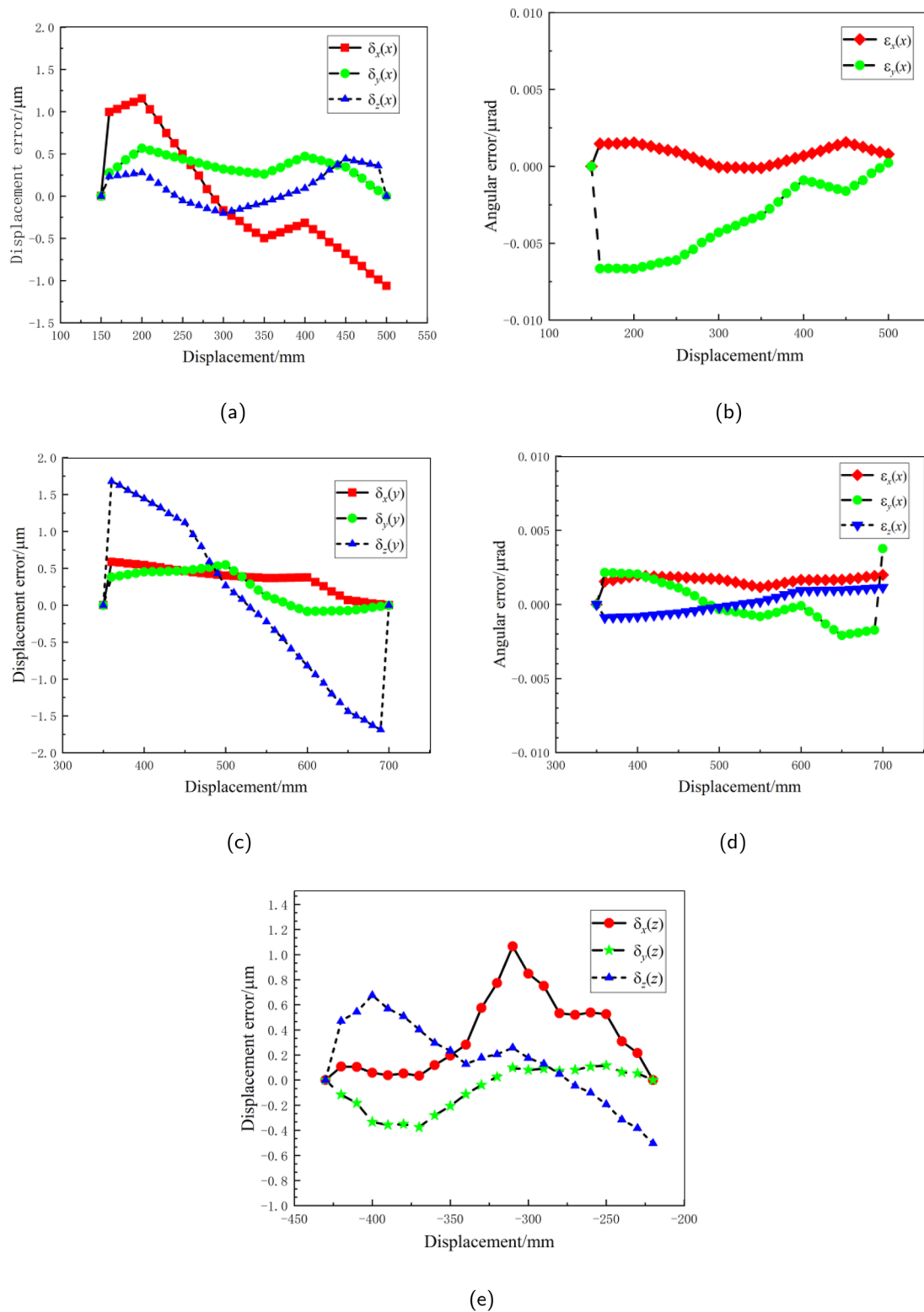


FIG. 5. Geometric errors. (a) X-axis positioning and straightness errors, (b) X-axis angular error, (c) Y-axis positioning and straightness errors, (d) Y-axis angular error, and (e) Z-axis positioning and straightness errors.

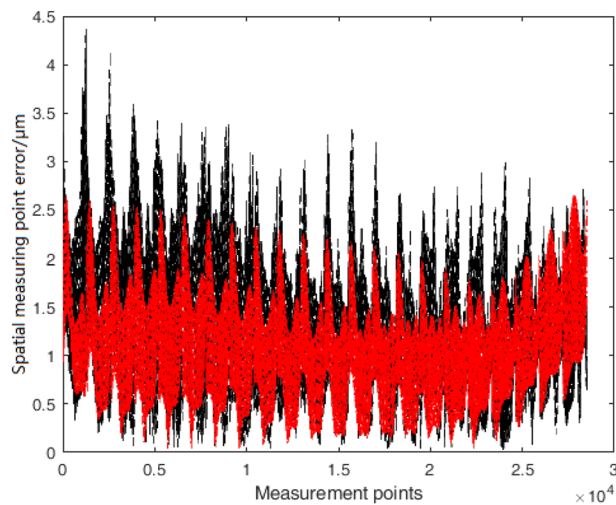


FIG. 6. Comparison chart of measurement point errors.

black curves indicate the errors in the measurement points obtained by interpolating the experimental data. The red curves indicate the errors obtained by substituting the coordinate values of the measurement points obtained via interpolation into the measurement point error model. The constructed measurement point error model was consistent with the actual error distribution pattern, thereby confirming the validity of the established CMM measurement point error model. Different measurement point errors were obtained. The experimental results were affected by motion errors, mechanism

errors, thermal errors, and environmental factors, whereas the constructed measurement point error model considered motion errors other than the four angular errors.

The measurement points obtained using the IDW interpolation method were substituted into the CMM measurement point error model to calculate the error of each measurement point. The distribution patterns of the measurement point errors in the working space are shown in Fig. 7. The measurement point errors varied with location in the CMM measurement space, suggesting that an optimal measurement area existed.

6. Particle swarm algorithm-based identification of optimal measurement area of CMM

Using the measurement point error model of the CMM established above, the optimal measurement area was identified using the particle swarm algorithm. In this study, the particle swarm algorithm is used to search for an optimal solution in a three dimensional search space. The dimensionality of the search space is three-dimensional, and the position of each particle represents a point in the search space. The search is achieved by updating the velocity and position of the particle. The particles are encoded in a continuous manner, meaning that the position of each particle is a three-dimensional vector. The parameters of the particle swarm algorithm were set as follows: population size (popsize = 35), maximum number of iterations (maxgen = 80), and search speed limit ($v = 3$). In addition, dynamic parameters were adopted: learning factor ($C_1 = C_2 = [0.5, 0.25]$), inertia weight ($\omega = [0.7, 1.4]$), and boundary conditions ($35 \times 35 \times 35$) mm³. By partitioning this space, 18 432 3D measurement spaces were obtained. The algorithm is evaluated for optimality by calculating the objective function. The smaller the value of the objective function, the better the particle is. The particle swarm optimization algorithm iterates, updated with

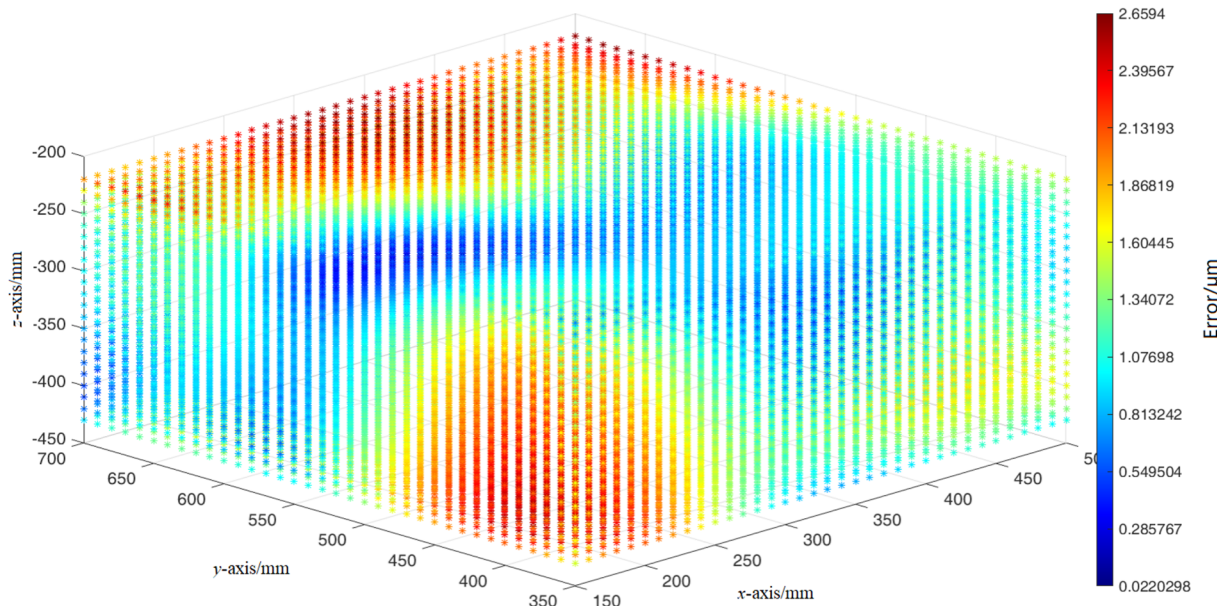


FIG. 7. Error distribution of measurement points with specified steps in the established measurement space.

the position and velocity of each particle, until certain stopping conditions are met. Eventually, the algorithm returns the optimal solution, obtaining the minimum value of the objective function and the optimal measurement interval. The maximum measurement point error for each measured space was determined using the particle swarm algorithm. The maximum measurement point error ranged from 0.34 to 2.66 μm . The comparison results of the maximum measurement point errors in different measurement areas confirmed the validity of the identification method for the optimal measurement area proposed herein. The data were selected at certain intervals to demonstrate the most significant difference in the maximum error of the measurement points in different measurement areas. In the measurement space planned by CMM, certain areas are selected arbitrarily, and the maximum error of the measured points in the selected area is calculated. The data for the maximum errors at certain measurement points are listed in **Table III**.

As shown in **Table III**, for the CMM measurement range set in this study, the minimum measurement point error was 0.34 μm . The area with the minimum measurement point error showed the following measurements: 280 mm < X < 315 mm, 540 mm < Y < 575 mm, and -400 mm < Z < -365 mm. This area was the optimal measurement area for the CMM in this study.

Using the proposed identification method, the measurement space can be flexibly partitioned based on the workpiece size and

actual operating conditions. Therefore, the proposed method for identifying the optimal measurement area exhibits high practicality and portability.

7. Comparison experiments

The experimental platform used for the comparison is shown in **Fig. 2**. A standard sphere was used as the measured object to validate the particle swarm algorithm-based identification method for the CMM optimal measurement area. A schematic illustration of the standard sphere measurement method is shown in **Fig. 8**. In the CMM measurement space, a standard sphere was placed at the position where the maximum measurement point error in the optimal measurement area was identified using the particle swarm algorithm. The spherical surface of the same standard sphere was measured to obtain the maximum error of the measurement points in different areas.

The planned spatial range of the CMM measurement is (350 \times 350 \times 210) mm³, according to Sec. VI B 1. The volumetric errors of 28 512 measurement points $E(x_i, y_i, z_i)$ ($i = 1, 2, 3, \dots, n$, $n = 28\,512$) planned in the CMM measurement space at a specified step size were obtained using the IDW interpolation method of Sec. VI B 6. Set $\bar{E}(x_i, y_i, z_i)$ to represent the mean value of the volumetric error at the CMM spatial measurement point. The $\bar{E}(x_i, y_i, z_i)$ obtained by IDW interpolation in Sec. VI B 6 of this paper

TABLE III. Maximum errors of measurement points in certain measurement areas.

Serial number	X-axis range (mm)	Y-axis range (mm)	Z-axis range (mm)	Location of maximum measurement point error (mm)	Maximum error (μm)
1	280–315	540–575	-400–-365	(315 540, -392.4915)	0.34
2	320–355	490–525	-390–-355	(321.593 751 7, -357)	0.36
3	340–375	460–495	-340–-305	(340 495, -305)	0.46
4	440–475	610–645	-280–-245	(444.822 161 0, -280)	0.49
5	260–295	460–495	-340–-305	(295 495, -305)	0.52
6	420–455	610–645	-420–-385	(455 645, -388.1828)	0.60
7	400–435	590–625	-260–-225	(435 590, -260)	0.64
8	220–255	490–525	-390–-355	(254.675 252 0, -366)	0.67
9	260–295	410–445	-270–-235	(295 445, -242.5609)	0.73
10	170–205	650–685	-400–-365	(189.652 765 0, -400)	0.96
11	440–475	660–695	-260–-225	(446.131 566 0, -260)	1.00
12	240–275	520–555	-290–-255	(240 532.0294, -261.9361)	1.02
13	150–185	410–445	-270–-235	(150 445, -235)	1.07
14	260–295	510–545	-310–-275	(265.786 252 8.8577, -275)	1.12
15	450–485	660–695	-410–-375	(485 695, -394.9558)	1.16
16	270–305	470–505	-400–-365	(270 470, -400)	1.41
17	370–405	480–515	-370–-335	(370 515, -335)	1.48
18	220–255	360–395	-410–-375	(252 364.7147, -379)	1.54
19	410–445	380–415	-400–-365	(410 380, -365)	1.56
20	210–245	630–665	-430–-395	(210 633.4061, -430)	1.66
21	220–255	390–425	-390–-355	(247.723 041 7, -358)	1.73
22	270–305	400–435	-430–-395	(270 413.2762, -430)	1.83
23	240–275	400–435	-380–-345	(240 405.7676, -380)	2.06
24	220–255	380–415	-400–-365	(220 407.7135, -400)	2.35
25	260–295	370–405	-430–-395	(189.473 240 5, -430)	2.66

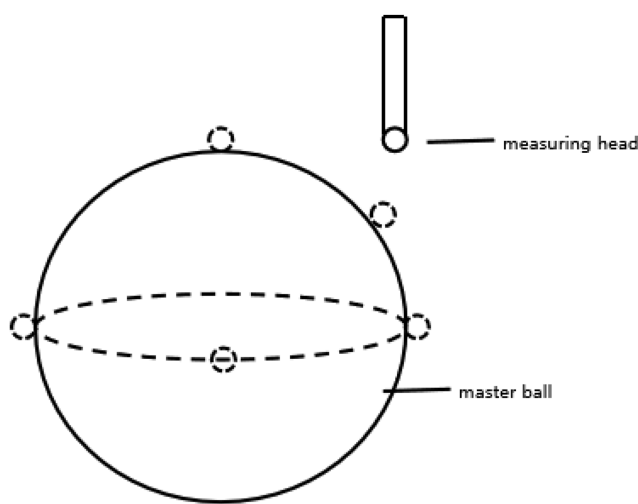


FIG. 8. Schematic diagram of standard sphere measurements.

is 1.1438×10^{-3} mm. In order to effectively cover the planned 28 512 measurement points in the CMM measurement space to a 95% confidence level, the limiting error $e = 5.7191 \times 10^{-5}$ mm for the volume error of the planned measurement points was obtained.

According to the formula for calculating the sample size for simple random sampling with no repeated sampling,²⁴ the limiting error formula is

$$e = Z \cdot S = Z \frac{\sigma}{\sqrt{N}}, \quad (37)$$

where e is the limiting error, Z is the probability density, S is the standard deviation estimate, σ is the standard deviation, and N is the sample size required for non-repeat sampling.

The standard deviation is calculated as follows:

$$\sigma = \sqrt{\frac{\sum_{i=1}^n [E(x_i, y_i, z_i) - \bar{E}(x_i, y_i, z_i)]^2}{n-1}}. \quad (38)$$

TABLE IV. Maximum errors of measurement points in certain areas.

Serial number	X-axis range (mm)	Y-axis range (mm)	Z-axis range (mm)	Location of maximum measurement point error (mm)	Experimental measurement error maximum (mm)
1	280–315	540–575	−400–−365	(315 540, −392.4915)	0.9361
2	420–455	610–645	−420–−385	(455 645, −388.1828)	0.9370
3	170–205	650–685	−400–−365	(189.652 765 0, −400)	0.9418
4	450–485	660–695	−410–−375	(485 695, −394.9558)	0.9443
5	270–305	470–505	−400–−365	(270 470, −400)	0.9467
6	210–245	630–665	−430–−395	(210 633.406 1, −430)	0.9542
7	270–305	400–435	−430–−395	(270 413.276 2, −430)	0.9612
8	240–275	400–435	−380–−345	(240 405.767 6, −380)	0.9660
9	220–255	380–415	−400–−365	(220 407.713 5, −400)	0.9713
10	260–295	370–405	−430–−395	(189.473 240 5, −430)	0.9745

According to Eq. (38), the standard deviation of the volumetric error of the measurement points for the IDW interpolation planning in Sec. VI B 6 of this paper is obtained as $\sigma = 1.8569 \times 10^{-3}$ mm.

When unduplicated sampling is used, the standard deviation estimate S of the sample size mean is

$$S = \sqrt{\frac{\sigma^2}{N} \left(1 - \frac{N}{n}\right)}. \quad (39)$$

According to Eqs. (37)–(39), the sample size N required for non-repetitive sampling, that is, the number of measurement points required for experimental validation, is obtained by

$$N = \frac{Z^2 \sigma^2 n}{e^2 n + Z^2 \sigma^2}. \quad (40)$$

At a confidence level of 95%, $Z = 1.96$. According to Eq. (40), the sample size N required for unduplicated sampling is 3547.

Therefore, in order to achieve a 95% confidence level in effectively covering 28 512 measurement points in the planned measurement space, randomly, $N = 3547$ measurement points are sampled in the CMM planned measurement space and measured using the CMM. The volumetric error of each measurement point is then calculated.

According to Sec. VI B 6, within the measurement space range (350 × 350 × 210) mm³ planned by the CMM, 600 3D subspaces (35 × 35 × 35) mm³ are included. 3547/600 ≈ 6 measurement points are randomly selected for the same standard sphere in a subspace to characterize the distribution of the volumetric errors in individual subspaces, which are then measured and compared with the volumetric errors.

The standard sphere was measured six times at locations with maximum errors in different areas. The accuracy of the proposed method was experimentally verified (Table IV). In the experimental data, the maximum error of the measurement point in the best measurement area is 0.9361 mm. After compensating for the height error of the magnetic base and the lifting platform, the maximum error value of the measurement point in this area is 0.0041 mm.

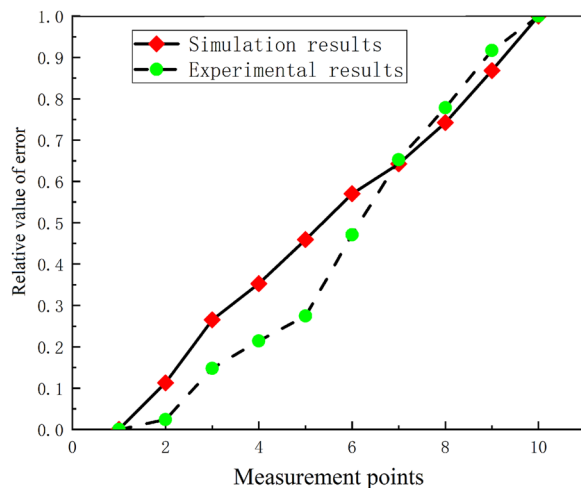


FIG. 9. Comparison of maximum errors of measurement points in some areas.

The experimental results show that the maximum measurement point error varied with the measurement area. However, the actual maximum errors in the different measurement areas differed from those identified by the algorithm. The algorithm simulation results and experimental measurements were standardized and normalized (Fig. 9) to verify the identification method for the optimal measurement area of the CMM proposed herein. The maximum errors of the measurement points in different areas solved by the algorithm were consistent with the experimental results. Therefore, the accuracy of the identification method for the optimal measurement area of the CMM proposed herein was verified.

The discrepancies between the maximum measurement point errors identified using the particle swarm algorithm and experimental results can be interpreted as follows:

- (1) The quasi-rigid body model is an ideal model that does not consider many factors, such as ambient temperature and mechanism error, which results in discrepancies between the solved geometric errors and actual results.
- (2) The four angular errors were disregarded. Only 17 geometric errors were considered in the modeling of the measurement point errors.
- (3) The installation error of the standard sphere and the experimental errors resulted in numerical differences between the experimental and algorithmic simulation results.

VII. CONCLUSION

In this study, the spatial error distribution pattern of CMM measurements was systematically investigated. The error distribution pattern was not uniform in different areas of the CMM measurement space, suggesting that an optimal measurement area with minimum error existed. The optimal measurement area was identified using the proposed method. The comparison experiments confirmed that the optimal measurement area identified using the

particle swarm algorithm was consistent with the actual measurements. Thus, the accuracy of the proposed method for determining the optimal measurement area of the CMM was verified.

In the future, we will identify the optimal measurement area for complex objects such as lines, circles, and spheres and extend the application scope of the proposed method to CMM with different traversal distances and accuracies. Based on the actual measurement requirements and existing measurement accuracy, different sizes of measured objects can be placed in the optimal measurement area to improve the accuracy of the measurement results.

ACKNOWLEDGMENTS

This research was supported by the National Natural Science Foundation of China (NSFC) under Grant Nos. 52175491 and 52227809.

AUTHOR DECLARATIONS

Conflict of Interest

The authors have no conflicts to disclose.

Author Contributions

Hongfang Chen: Conceptualization (equal); Funding acquisition (equal); Methodology (equal); Resources (equal); Validation (equal). **Huan Wu:** Data curation (equal); Investigation (equal); Software (lead); Validation (equal); Writing – review & editing (lead). **Yi Gao:** Data curation (lead); Software (lead); Writing – original draft (lead). **Zhaoya Shi:** Funding acquisition (equal). **Zhongpu Wen:** Supervision (equal). **Ziqi Liang:** Supervision (equal); Writing – review & editing (equal).

DATA AVAILABILITY

The data that has been used is confidential.

REFERENCES

- ¹Z. Y. Shi, B. Zhang, J. C. Lin, and H. Zhang, “Half century of coordinate metrology technology—Evolution and trend,” *J. Beijing Univ. Technol.* **37**(5), 648–656 (2011).
- ²Compiled by Hexagon Measurement Technology LTD, *Practical Coordinate Measurement Technology* (Chemical Industry Press, 2007).
- ³J. Zhou, L. Y. Zheng, W. Fan, and Y. S. Cao, “Intelligent hierarchical compensation method for industrial robot positioning error based on compound branch neural network automatic creation,” *J. Intell. Manuf.* (published online) (2024).
- ⁴Y. Li, B. Li, X. Zhao, S. M. Cheng, W. Zhang, and W. Tian, “Error similarity analysis and error compensation of industrial robots with uncertainties of TCP calibration,” *Appl. Sci.* **13**(4), 2722 (2023).
- ⁵D. D. Chen, T. M. Wang, P. J. Yuan, N. Sun, and H. Y. Tang, “A positional error compensation method for industrial robots combining error similarity and radial basis function neural network,” *Meas. Sci. Technol.* **30**(12), 125010 (2019).
- ⁶L. Li, H. Yang, L. Jiang, J. Gu, and Y. Zhang, “Optimal measurement area determination algorithm of articulated arm measuring machine based on improved FOA,” *Meas. Control* **53**(9–10), 2146–2158 (2020).
- ⁷M. Uekita and Y. Takaya, “On-machine dimensional measurement of large parts by compensating for volumetric errors of machine tools,” *Precis. Eng.* **43**, 200–210 (2016).

- ⁸G. Moona, V. Kumar, M. Jewariya, H. Kumar, and R. Sharma, "Measurement uncertainty assessment of articulated arm coordinate measuring machine for length measurement errors using Monte Carlo simulation," *Int. J. Adv. Des. Manuf. Technol.* **119**(9–10), 5903–5916 (2022).
- ⁹D. T. Zheng, C. T. Du, and Y. G. Hu, "Research on optimal measurement area of flexible coordinate measuring machines," *Measurement* **45**(3), 250–254 (2012).
- ¹⁰H. Yi, J. Chao, H. Wei, and P. H. Hu, "Optimal measurement area of articulated coordinate measuring machine calculated by ant colony algorithm," *Opt. Precis. Eng.* **25**(6), 1486–1493 (2017).
- ¹¹H. T. Yang, Q. Ma, Y. Zhang, L. Li, M. Shen, and J. Wang, "Research on the method of determining the best measuring area for the circular surface survey," *Int. J. Adv. Des. Manuf. Technol.* **118**(9–10), 3457–3475 (2022).
- ¹²K. I. Lee, J. C. Lee, and S. H. Yang, "Optimal on-machine measurement of position-independent geometric errors for rotary axes in five-axis machines with a universal head," *Int. J. Precis. Eng. Manuf.* **19**(4), 545–551 (2018).
- ¹³T. Mazur, L. Cepova, T. Szymanski, and M. Rucki, "Analysis of the planar point identification accuracy in CMM measurements," *Sensors* **22**(18), 7005 (2022).
- ¹⁴V. Trivedi, P. Varshney, and M. Ramteke, "A simplified multi-objective particle swarm optimization algorithm," *Swarm Intell.* **14**(6), 83–116 (2019).
- ¹⁵X. L. Shu, Y. M. Liu, J. Liu, M. L. Yang, and Q. Zhang, "Multi-objective particle swarm optimization with dynamic population size," *J. Comput. Des. Eng.* **10**(1), 446–467 (2023).
- ¹⁶G. X. Zhang, *Coordinate Measuring Machines* (Tianjin University Press, Tianjin, 1999).
- ¹⁷H. F. Chen, B. W. Zheng, Z. Y. Shi, Y. Q. Sun, C. Y. Long, and Z. H. Yang, "CMM spatial coordinate correction method based on laser tracker multi-station measurement," *Chin. J. Lasers* **44**(3), 197–204 (2017).
- ¹⁸C. F. Ma, *Optimization Method and MATLAB Program Design* (Science Press, 2010).
- ¹⁹M. Azeem, S. Hussain, M. Ijaz, N. Salahuddin, and A. Salam, "An improved version of systematic sampling design for use with linear trend data," *Heliyon* **9**(6), 17121 (2023).
- ²⁰H. F. Chen, S. Zhang, C. W. Liang, L. Tang, and Z. Y. Shi, "Method for volume error calibration of CMM based on inverse-distance weighting algorithm," *Chin. J. Lasers* **47**(12), 144–153 (2020).
- ²¹H. F. Chen, S. Zhang, G. Y. Wang, Y. Gao, M. Y. Sun, W. G. Lu, H. X. Song, and Z. Y. Shi, "LASSO based compensation method for geometric errors of large coordinate measuring machine," *Measurement* **196**, 111157 (2022).
- ²²J. Kennedy and R. Eberhart, "Particle swarm optimization," in *Proceedings of the IEEE International Conference on Neural Networks* (IEEE, 1995), Vol. 4, pp. 1942–1948.
- ²³B. Daniel and J. Kennedy, "Defining a standard for particle swarm optimization," in *2007 IEEE Swarm Intelligence Symposium* (IEEE, 2007), pp. 120–127.
- ²⁴A. Riaz, M. N. Amin, W. Emam, Y. Tashkandy, U. Yasmeen, J. Rahimi, *Sci. Rep.* **13**(1), 17617 (2023).